Mode-coupling theory and polynomial fitting functions: A complex-plane representation of dielectric data on polymers

H. Eliasson
Department of Experimental Physics, Physics and Engineering Physics, Göteborg University and Chalmers University of Technology, SE-412 96 Göteborg, Sweden

(Received 29 November 2000; published 14 June 2001)

Recently, it has been shown that the higher-order A_3 and A_4 scenarios of the mode-coupling theory (MCT) are in many cases capable of providing a good description of the complicated dielectric spectra often encountered in polymeric systems. In this paper, more data from dielectric measurements on poly(ethylene terephthalate), poly(vinylidene fluoride), Nylon-66, poly(chlorotrifluoroethylene) (PCTFE), and the polymer gel system poly(acrylonitrile)–ethylene carbonate–propylene carbonate are evaluated within the A_4 scenario of the MCT. For all these systems, very good agreement is found between the theoretical and experimental spectra. The data analysis is demonstrated to be facilitated considerably by plotting the data in the complex plane whereby the elliptic functions derived from the theory for the frequency-dependent dielectric function can be replaced by polynomials. For PCTFE, the scaling behavior predicted by the MCT could be verified and the temperature dependences of the extracted scaling parameters were found to be consistent with theory.

DOI: 10.1103/PhysRevE.64.011802 PACS number(s): 61.41.+e, 77.22.Gm, 64.70.Pf

I. INTRODUCTION

Dielectric data obtained from measurements on polymers often show very complex relaxation patterns. The usual way to analyze such data has to date been to use various semiempirical expressions, for instance, the Cole-Cole [1], Cole-Davidson [2,3], or Havriliak-Negami [4] functions. These expressions can account for features such as broadened and asymmetric loss peaks, typical for many simple glass-forming materials. In amorphous and semicrystalline polymers, however, the frequency-dependent imaginary part of the dielectric function $\epsilon''(\nu)$ often features frequency-independent regions, linear regions in $\ln(\nu)$, horizontal inflection points, or double minima [5–16]. In these cases, the above formulas, in general, do not provide an adequate description of the data. Rather recently, however, this behavior has been demonstrated to be described astonishingly well using the higher-order scenarios within the mode-coupling theory (MCT) of the liquid-glass transition [11–17]. However, even though the theoretical expressions do show good correspondence with measured data, it has, due to the multidimensional nature of the problem, not yet been possible to thoroughly test the scaling relations predicted by the theory. Therefore, one purpose of this paper is to present more data supporting the theory, which also illustrates the scaling properties. Furthermore, applying this theory to the analysis of frequency-domain data involves the use of elliptic functions that cannot be calculated analytically. The ''catastrophic'' behavior of these functions, as well as their strong divergence at low and high frequencies, makes it quite difficult to utilize automated curve fitting procedures. Due to this and to the large amount of data needed, analysis of data using the higher-order scenarios of the MCT has thus far been a quite cumbersome and tedious affair. Another purpose of this paper is therefore to present a simpler way to analyze dielectric data on polymers within the framework of the MCT, which allows for the use of simple polynomial functions and thus permits linear least squares curve fitting to be utilized. For this purpose, the following polymeric systems were chosen: poly(ethylene terephthalate) (PET), poly(chlorotrifluoroethylene) (PCTFE), poly(vinylidene fluoride) (PVDF), poly(hexamethylene adipamide) (Nylon-66), and the polymer gel system poly(acrylonitrile)–ethylene carbonate–propylene carbonate (PAN-EC-PC). The paper is organized as follows. In Sec. II a brief introduction to dielectric data analysis is presented, followed by a description of the mode-coupling theory in Sec. III, where all relevant formulas and expressions are introduced. Results of the polynomial curve fits are shown in Sec. IV. In order to demonstrate the validity of the polynomial fits, the dielectric spectra are also fitted to the ''usual'' elliptic functions using the parameters obtained from the polynomial fits. Finally, the paper is concluded in Sec. V with a discussion of the results.

II. PRESENTATION OF DIELECTRIC DATA

The data obtained from a dielectric experiment can be represented in a number of ways. Today, it is most common to plot the real and imaginary parts of the dielectric function $\epsilon(\nu)=\epsilon'(\nu)-i\epsilon''(\nu)$ as separate functions of the frequency ν. In such a plot the relaxations found in the material will show up as peaks in the imaginary part ϵ'', accompanied by a step in the real part ϵ'. Another method to present the data is the Cole-Cole plot [1]. Here, ϵ'' is plotted as a function of ϵ' in a complex-plane representation. In the simplest theory [18,19], where the relaxation function in the time domain is modeled by an exponential decay and $\epsilon(\nu)\propto(1+i2\pi\nu\tau)^{-1}$, such a plot will give rise to a semicircle centered on the real axis. In reality, and especially in the case of polymers, this is seldom seen but the semicircle appears distorted and is often not visible in its entirety.

III. MODE-COUPLING THEORY

During recent years, the mode-coupling theory [20] has emerged as a very promising theoretical framework for de-

scribing the dynamics of glass-forming systems. Today, many experimental studies have confirmed the predictions of the theory for a large number of materials [21]. A central concept in the MCT is that of glass transition singularities. Due to the fact that the MCT equations cannot be solved exactly, approximations are employed, either through the use of so-called schematic models or by asymptotic expansions. In the present case, the latter method has been adopted, implying that the equations presented below are only applicable close to the relevant singularity and in an intermediate frequency range called the β-relaxation region, located between the structural α-relaxation and higher-frequency microscopic processes. The theory predicts a critical temperature T_c, which represents a transition from liquidlike dynamical behavior for $T>T_c$ to solidlike behavior for $T\leqslant T_c$. Because of the asymptotic nature of the solutions to the MCT equations, the abovementioned singularities manifest themselves in a number of different scenarios and are classified according to results from catastrophe theory [22,23]. In the simplest case, the A_2 scenario, the imaginary part of the dielectric function is in the β-relaxation region above T_c given by a minimum centered at $(\nu_{\min},\epsilon''_{\min})$, which is formed by two power laws according to

$$\epsilon''(\nu)=\frac{\epsilon''_{\min}}{a+b}\left[b\left(\frac{\nu}{\nu_{\min}}\right)^a+a\left(\frac{\nu_{\min}}{\nu}\right)^b\right] \tag{1}$$

and whose exponents a and $-b$ are related to each other and to a material-dependent exponent parameter λ according to

$$\lambda=\frac{\Gamma^2(1-a)}{\Gamma(1-2a)}=\frac{\Gamma^2(1+b)}{\Gamma(1+2b)}, \tag{2}$$

where $\Gamma(x)$ is the gamma function. For temperatures below T_c, the power law with exponent $-b$ is replaced by a white-noise spectrum, $\epsilon''(\nu)\propto\nu^1$.

A. Higher-order scenarios and elliptic functions

For many polymers, the A_2 scenario cannot adequately explain the very complex relaxation patterns encountered sometimes. Furthermore, the MCT predicts the A_2 scenario to break down when λ approaches unity. When this happens, higher-order scenarios must be used. For these, the general expressions for the real and imaginary parts of the dielectric function can be written in leading order as

$$\epsilon'(\nu)=f_\epsilon-\epsilon_c f(y;g_2,g_3,\ldots,g_k), \tag{3a}$$

$$\epsilon''(\nu)=-\frac{\pi}{2}\epsilon_c f'(y;g_2,g_3,\ldots,g_k), \tag{3b}$$

where $y=-\ln(2\pi\nu t_1)$, f_ϵ and ϵ_c are fitting parameters, $f'(y)=df/dy$, and t_1 is a characteristic microscopic timescale [11,12]. The parameters g_ℓ ($\ell=2,3,\ldots$) are mathematical control parameters and specify the distance to the relevant singularity in such a way that the singularity is reached when $g_2=g_3=\cdots=g_k=0$. These parameters control the shape of the dielectric function. The function $f(y)$ is determined from the differential equation [17]

$$\left(\frac{df}{dy}\right)^2=S_k(f(y)) \tag{4}$$

where $k\geqslant 3$ and $S_k(x)$ is a polynomial given by

$$S_k(x)=\frac{4}{(k-2)^2}x^k-g_2x^{k-2}-\cdots-g_{k-1}x-g_k. \tag{5}$$

The solutions to these equations are expressed in terms of elliptic functions. In case of the A_3 singularity, for which $k=3$, the function $f(y)$ is given by the Weierstrass elliptic function $\wp(y;g_2,g_3)$ [11,17], which can be calculated via the elliptic integral

$$y=\int_\wp^\infty\frac{ds}{\sqrt{4s^3-g_2s-g_3}}. \tag{6}$$

There are thus two shape parameters, g_2 and g_3, in this case. The next higher-order scenario, the A_4 scenario [12] has three shape parameters, g_2, g_3, and g_4, and the function $f(y)$ can be calculated through

$$y=\int_f^\infty\frac{ds}{\sqrt{s^4-g_2s^2-g_3s-g_4}}. \tag{7}$$

In the frequency domain, all these higher-order scenarios provide their own very specific signatures. For instance, the A_3 scenario introduces a horizontal inflection point in $\epsilon''(\nu)$, while the A_4 scenario in addition exhibits, e.g., double minima and regions linear in $\ln(\nu)$. For all higher-order singularities A_k, $k\geqslant 3$, lower-order singularities appear as special limits, determined by the number of degenerate roots of the polynomial $S_k(x)$. The A_2 singularities are encountered when two degenerate roots are found, while the set of A_3 singularities is found for all cases where the polynomial $S_k(x)$ has three coalescent roots and so on.

B. Parameter spaces

By considering the control parameters g_ℓ, $\ell=2,3,\ldots,k$, to be coordinates in a $(k-1)$-dimensional space, each measured spectrum will correspond to a point in this space. When varying physical parameters such as, e.g., temperature, pressure, or composition, the set of points thus acquired will form a path. This path may cross critical lines or surfaces containing the A_2 singularities. If that happens, a transition is predicted to take place between a liquid state and an ideal glass state (the transition takes place at the temperature $T=T_c$) or, as could be the case for the A_4 and higher scenarios, between two ideal glass states. Since the set of A_2 singularities is determined by establishing for which values of the parameters g_ℓ the polynomial $S_k(x)$ has roots of twofold degeneracy [22,23], the critical lines or surfaces can be determined through the identities

$$S_3(x)=4x^3-g_2x-g_3=(x-x_{0,3})^2(x-x_{1,3})=0 \tag{8a}$$

for the A_3 scenario and

$$S_4(x)=x^4-g_2x^2-g_3x-g_4=(x-x_{0,4})^2(x-x_{1,4})(x-x_{2,4})$$
$$=0 \tag{8b}$$

for the A_4 scenario. Here, $\{x_{l,k}\}$ are the roots of the polynomial $S_k(x)$. By identification, the critical line (in the A_3 case) or surface (for the A_4 scenario) are then given by the parametric representations

$$g_2=12x_0^2, \tag{9a}$$

$$g_3=-8x_0^3 \tag{9b}$$

for the A_3 case, where $x_0\in[0,\infty)$ and

$$g_2=(x_0+x_1)^2+2x_0^2, \tag{10a}$$

$$g_3=-2x_0(x_0+x_1)^2, \tag{10b}$$

$$g_4=x_0^2x_1(2x_0+x_1) \tag{10c}$$

for the A_4 scenario. These last three relations may be more conveniently expressed as

$$g_3=-2x_0(g_2-2x_0^2), \tag{10d}$$

$$g_4=x_0^2(g_2-3x_0^2) \tag{10e}$$

for $g_2\in(-\infty,\infty)$ and $x_0\in\{(-\infty,-\sqrt{g_2/2}],[\sqrt{g_2/6},\infty)\}$, for $g_2\geqslant 0$ and $x_0\in(-\infty,\infty)$ otherwise. In the same way, the set of A_3 singularities will in the A_4 case be given by a line in the (g_2,g_3,g_4) parameter space described by the following parametric functions:

$$g_2=6x_0^2, \tag{11a}$$

$$g_3=-8x_0^3, \tag{11b}$$

$$g_4=3x_0^4, \tag{11c}$$

where $x_0\in[0,\infty)$.

C. Scaling relations

The elliptic functions $f(y;g_2,g_3,\ldots,g_k)$ are homogeneous, i.e., they can be rescaled according to [11,12]

$$f(y;g_2,g_3,\ldots,g_k)=s^nf(ys;g_2s^{-2n},g_3s^{-3n},\ldots,g_ks^{-kn}), \tag{12}$$

where $n=2/(k-2)$. As a consequence, the expressions for the dielectric function in the A_3 and A_4 scenarios can, by letting $s=|g_3/4|^{1/6}$ in the A_3 case [11] and $s=|g_4/3|^{1/4}$ for the A_4 singularity [16,27], alternatively be written as

$$\epsilon'(\nu)=f_\epsilon-c'_\xi\wp\left(\frac{y}{y_\xi};\pm 12\left(\frac{r}{4}\right)^{1/3},\pm 4\right), \tag{13a}$$

$$\epsilon''(\nu)=-c''_\xi\wp'\left(\frac{y}{y_\xi};\pm 12\left(\frac{r}{4}\right)^{1/3},\pm 4\right) \tag{13b}$$

for the A_3 singularity [11] and as

$$\epsilon'(\nu)=f_\epsilon-c'_4f\left(\frac{y}{y_4};\pm 6p^{1/2},\pm 8q^{1/4},\pm 3\right), \tag{14a}$$

$$\epsilon''(\nu)=-c''_4f'\left(\frac{y}{y_4};\pm 6p^{1/2},\pm 8q^{1/4},\pm 3\right) \tag{14b}$$

in the A_4 scenario. The parameters r, p, and q will then be given by

$$r=\left|\frac{g_2^3}{27g_3^2}\right|, \tag{15a}$$

$$p=\left|\frac{g_2^2}{12g_4}\right|, \tag{15b}$$

$$q=\left|\frac{27g_3^4}{4096g_4^3}\right|. \tag{15c}$$

There will thus exist lines in the $(k-1)$-dimensional parameter space along which the corresponding spectra are invariant. The parameters above have been defined so that $r=1$ is the equation of the A_2 line in the A_3 scenario, while $p=q=1$ corresponds to the A_3 line in the three-dimensional A_4 parameter space. This scaling property leads to the prediction that the parameters in Eqs. (13) and (14) should have the following temperature dependences:

$$\frac{c'_\xi}{\epsilon_c}\propto\left|\frac{T_0-T}{T_0}\right|^{1/3}, \tag{16a}$$

$$\frac{c''_\xi}{\epsilon_c}\propto\left|\frac{T_0-T}{T_0}\right|^{1/2}, \tag{16b}$$

$$\frac{1}{y_\xi}\propto\left|\frac{T_0-T}{T_0}\right|^{1/6}, \tag{16c}$$

$$\frac{c'_4}{\epsilon_c}\propto\left|\frac{T_0-T}{T_0}\right|^{1/4}, \tag{17a}$$

$$\frac{c''_4}{\epsilon_c}\propto\left|\frac{T_0-T}{T_0}\right|^{1/2}, \tag{17b}$$

$$\frac{1}{y_4}\propto\left|\frac{T_0-T}{T_0}\right|^{1/4}. \tag{17c}$$

T_0 is here the temperature at which the relevant singularity is reached. Thus for spectra having similar r values (for the A_3 case) or p, q values (for the A_4 case), the extracted scaling parameters should show the above temperature dependence. This provides for a critical testing of the theory. In many cases, the parameter ϵ_c only shows a weak temperature dependence and is therefore usually absorbed by the parameters c' and c''. However, when performing a scaling analysis on polymers with, e.g., varying degree of crystallinity where the

intensities of the spectra vary to a much greater extent between samples, the influence of ϵ_c needs to be taken into account.

D. Polynomial representation of ϵ' and ϵ''

Due to the nature of the above described elliptic functions, automatic curve fitting procedures are very difficult to implement for the higher-order MCT scenarios. A different route can be taken by observing that ϵ'' is related to the derivative of the function $f(y)$ [13]. From Eqs. (3) and (4) one then finds that ϵ'' is related to ϵ' through the polynomial expression

$$\epsilon''^2 = \sum_{i=0}^{k} a_i \epsilon'^i \tag{18}$$

from which the various parameters from Eq. (3) can be extracted according to

$$\epsilon_c = -\frac{\pi^2}{a_3}, \tag{19a}$$

$$f_\epsilon = -\frac{a_2}{3a_3}, \tag{19b}$$

$$g_2 = \frac{4a_2^2 - 12a_1a_3}{3\pi^4}, \tag{19c}$$

$$g_3 = \frac{36a_1a_2a_3 - 8a_2^3 - 108a_0a_3^2}{27\pi^6} \tag{19d}$$

for the A_3 case ($k=3$) and

$$\epsilon_c = \frac{\pi}{2a_4^{1/2}}, \tag{20a}$$

$$f_\epsilon = -\frac{a_3}{4a_4}, \tag{20b}$$

$$g_2 = \frac{3a_3^2 - 8a_2a_4}{2a_4\pi^2}, \tag{20c}$$

$$g_3 = \frac{8a_1a_4^2 + a_3^3 - 4a_2a_3a_4}{a_4^{3/2}\pi^3}, \tag{20d}$$

$$g_4 = \frac{64a_1a_3a_4^2 - 16a_2a_3^2a_4 - 256a_0a_4^3 + 3a_3^4}{16a_4^2\pi^4} \tag{20e}$$

for the A_4 singularity ($k=4$). In this way, all parameters except the timescale t_1 can be determined by fitting a polynomial of order k to a plot of ϵ''^2 versus ϵ'. It is however important to realize that the accuracy of the MCT expressions for the dielectric function depends on the distance to the relevant singularity. This means that even though a very good fit is obtained with the polynomial expression, this is not necessarily carried over to the elliptic functions describing the real and imaginary parts, respectively. One of the purposes of this paper is to investigate in more detail the correspondence between the polynomial fits on the one hand and the elliptic functions on the other.

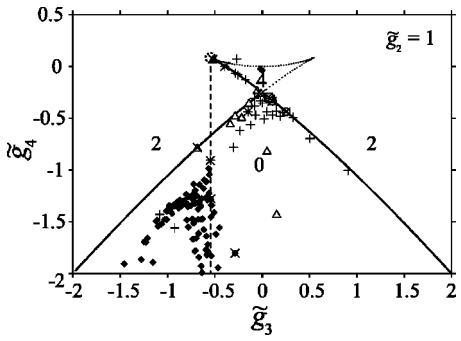

FIG. 1. Cut of the A_4 parameter space with the plane $\tilde{g}_2 = 1$, see text. Black diamonds, PAN-EC-PC; pluses, PET; triangles, PCTFE; circles, Nylon-66; squares, PVDF. Crosses mark the spectra that are plotted in the following figures. The dashed circle shows the location of the A_3 point, located at $(\tilde{g}_3, \tilde{g}_4) = (-(2/3)^{3/2}, 1/12)$ and the dashed line contains all parameter points that give rise to a horizontal inflection point in the polynomial $S_4(x)$. The numbers 0, 2, and 4 indicate the number of real roots of the polynomial S_4 in the relevant region.

It should be noted that the a_i parameters cannot be chosen arbitrarily since, e.g., a negative value of the parameter a_4 yields imaginary coefficients ϵ_c and g_3 in the A_4 case.

According to Eq. (12), the scaling relation for the $S_k(x)$ polynomial is given by

$$S_k(x; g_2, g_3, \ldots, g_k) = s^{kn} S_k(xs^{-n}; g_2 s^{-2n}, g_3 s^{-3n}, \ldots, g_k s^{-kn}). \tag{21}$$

For the A_4 scenario, which is the primary scenario of interest in the present work, the master functions along scaling lines given by constant p and q values do consequently have the following form:

$$\frac{\epsilon''}{c_4''} = \sqrt{S_4\left(\frac{f_\epsilon - \epsilon'}{c_4'}; \pm 6p^{1/2}, \pm 8q^{1/4}, \pm 3\right)} = \sqrt{\left(\frac{f_\epsilon - \epsilon'}{c_4'}\right)^4 \mp 6p^{1/2}\left(\frac{f_\epsilon - \epsilon'}{c_4'}\right)^2 \mp 8q^{1/4}\frac{f_\epsilon - \epsilon'}{c_4'} \mp 3}. \tag{22}$$

IV. RESULTS

The part of the A_4 parameter space relevant for the present case is shown in Fig. 1. The points represent the positions of the different fitted spectra within this space. Because of Eq. (21) and by choosing $s = |g_2|^{1/2}$ so that $\tilde{g}_3 = g_3/|g_2|^{3/2}$ and $\tilde{g}_4 = g_4/|g_2|^2$, this three-dimensional space is completely characterized by the three cuts with the planes

$g_2=-1$, $g_2=0$, and $g_2=1$. Since all the g_2 parameters obtained from the fits were positive, only the cut with the $g_2=1$ plane needs to be considered in the present case. The full lines are the sets of all A_2 singularities, calculated according to Eqs. (10d) and (10e), and do thus represent crossovers between different ideal glass states and between liquid and ideal glass states. The line starting from the A_3 point and extending downwards and to the right is divided into two parts. The upper part, between the A_3 point and the corner represents a glass-glass transition. The lower line represents a liquid-glass transition. The other line, starting from the corner and extending towards the lower left, represents the transition surface between liquid and ideal glass states. The dotted part of the critical surface, drawn to show the full ''swallowtail'' shape, represents an unphysical situation [12]. The dashed straight line that extends from the A_3 point and downwards contains the set of parameter points that produce a horizontal inflection point in the polynomial S_4. Some parameter points in the figure are marked with a cross. These represent typical results and the spectra corresponding to these points are plotted in the following figures.

PET is a polymer with a dielectric spectrum that shows an almost A_2-like behavior in the amorphous state close to the critical temperature T_c. Discrepancies between the A_2 scenario and experimental data for this polymer have however been found [14,24] and the reason for this deviation was explained by taking the A_3 singularity into account [14]. Dielectric data on PET with varying degree of crystallinity were also evaluated within the A_3 scenario with partial success [15]. These data have now been reevaluated within the A_4 scenario, the result of which is shown in Fig. 2 for a few representative spectra. The complex-plane analysis produces excellent fits that are easily carried over to the frequency-plane plots. It should be pointed out that for all the evaluated data, except when otherwise noted, the fitting parameters were obtained from fits using expressions (18), (19), and (20) and these parameters were then used to generate the elliptic functions in Eqs. (3). These plots also illustrate the fact that close to the A_3 points, as seen in Fig. 1, the A_3 and A_4 scenarios are equivalent. However, further away from the A_3 points deviations start to appear and the A_4 scenario provides a much better description of the data. In contrast with the A_2 scenario, which exclusively deals with the minimum between two peaks, the higher-order scenarios are also able to reproduce a large part of the α peak. This is due to the fact that the time-domain relaxation function for the higher-order scenarios is more slowly varying compared to the A_2 scenario and a larger part of the α peak will therefore be reproduced in these cases. Of particular interest is the fact that the α peak of the PET spectrum is not fitted to the low-frequency wing of the A_4 fitting curve but rather to the intermediate-frequency peak situated between the two minima as found in the liquid region beneath the corner in Fig. 1. This gives the result, as can be seen in Fig. 2, that another peak is predicted for frequencies below the α peak. On crossing the bifurcation surface extending from the corner towards the lower left in Fig. 1, this low-frequency peak will disappear. The α peak will however remain intact and will instead disappear when crossing the critical surface

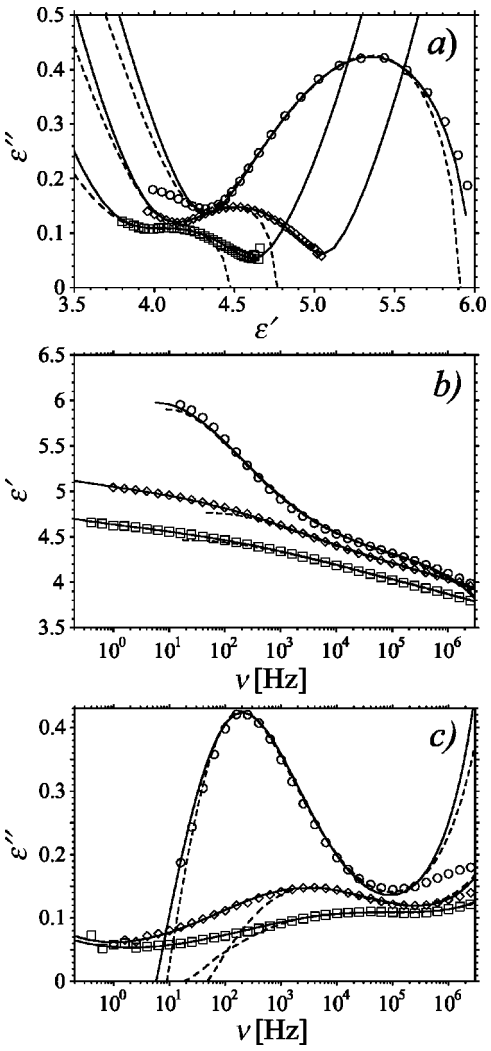

FIG. 2. MCT fits to the dielectric function for PET. Full lines are A_4 fits and dashed lines fits to the A_3 scenario, see text. (a) Complex-plane plot. (b) Real and (c) imaginary part of the dielectric function as functions of frequency ν. Circles, 9% crystallinity at 90 °C; diamonds, 26% crystallinity at 110 °C; squares, 31% crystallinity at 115 °C. In Fig. 1, the coordinates $(\tilde{g}_3,\tilde{g}_4)$ of these spectra are $(-0.39,6.7\times10^{-4})$, $(-0.15,-0.44)$, and $(-0.55,-0.91)$ and the g_2 parameters are 0.22, 0.047, and 0.022, respectively.

making up the left part of the ''swallowtail'' shape. This implies, as previously discussed by Fuchs *et al.* [26], a two-step glass transition scenario. For dielectric measurements, this prediction might be difficult to corroborate, since for low enough frequencies ϵ'' will start to increase due to electrode polarization and dc conductivity. The low-frequency peak, or α' peak, is actually found in dielectric spectra for, e.g., poly(propylene glycol) [25]. Using a schematic model, it has previously been shown by Fuchs *et al.* [26] that this double-peak scenario is indeed a generic feature of the MCT and appears close to the self-intersection of the critical surface. Thus, spectra located below and close to the corner with coordinates $(\tilde{g}_3,\tilde{g}_4)=(0,-1/4)$ in Fig. 1 will display such a double peak, or more accurately, a double minimum, since

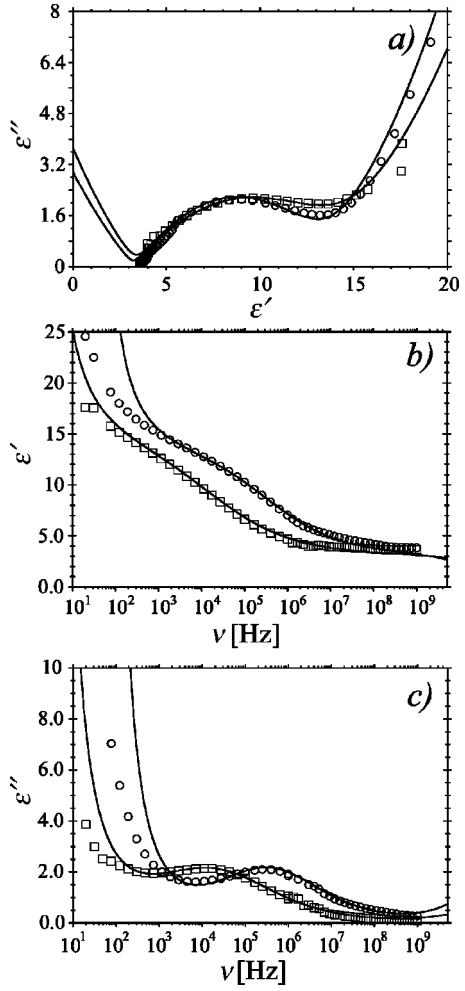

FIG. 3. MCT fits to the dielectric function for Nylon-66. Full lines are A_4 fits, see text. (a) Complex-plane plot, (b) real, and (c) imaginary part of the dielectric function plotted as functions of frequency ν. Squares, 47 °C; circles, 98 °C. In Fig. 1, the coordinates $(\tilde{g}_3,\tilde{g}_4)$ of these spectra are $(0.25,-0.44)$ and $(0.11,-0.34)$ and the g_2 parameters are 0.082 and 0.12, respectively.

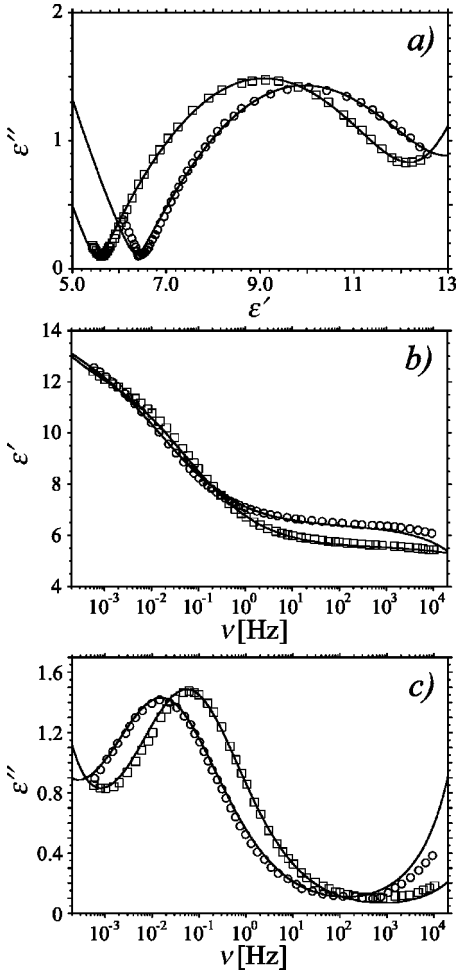

FIG. 4. MCT fits to the dielectric function of PVDF. Full lines are A_4 fits, see text. (a) Complex-plane plot, (b) real, and (c) imaginary part of the dielectric function plotted as functions of frequency ν. Circles, 0 °C; squares, 10 °C. In Fig. 1, the coordinates $(\tilde{g}_3,\tilde{g}_4)$ of these spectra are $(0.083,-0.31)$ and $(0.065,-0.30)$ and the g_2 parameters are 0.12 and 0.14, respectively.

only the high-frequency part of the lowest-frequency peak is visible due to the asymptotic nature of the A_4 scenario.

Figure 3 shows the results from fitting the A_4 functions to dielectric data taken from measurements on Nylon-66 [27]. Here the A_4 fits also produce very good results. However, for the low temperature sample the complex-plane fit produced parameter values that corresponded to a point on the right side of the rightmost critical line in Fig. 1. Attempting to produce an elliptic function that fitted the spectrum for the parameter values obtained from the polynomial fits did therefore not succeed in this case. This is due to the fact that there are not enough data on the high-frequency side of the spectrum that gives, as a result, a polynomial in ϵ' that will become negative and thereby exhibit two real roots. By visual inspection of the experimental spectra, one can however immediately conclude that this spectrum belongs to that part of the parameter space where the polynomial $S_4(x)$ has no real roots, since spectra in this region show an intermediate frequency peak or inflection point as well as the high-frequency side of a lower-frequency peak. By extrapolating the data in Fig. 3(a) with a few points at low values of ϵ', a successful polynomial fit was also accomplished for this case.

Like Nylon-66, dielectric data for PVDF also show typical A_4 behavior with a double minimum. The data shown in Fig. 4 were taken from the literature [28]. $\epsilon'(\nu)$ was not available from that report and was therefore calculated by performing a numerical Kramers-Kronig transformation according to a method developed by Lovell [29]. Apart from a wide frequency range, such an analysis requires that the value of ϵ' at infinitely high frequencies, ϵ_∞, be determined. Since this value is very dependent upon the degree of crystallinity and thermal history of the sample, a correct assessment of this parameter could not be made, and a reasonable estimate was determined to be $\epsilon_\infty=5$ [30–32]. Since ϵ_∞ is just an additive constant, it will only affect the value of f_ϵ when performing A_4 fits. The lowest temperature sample was also in this case giving problems for the complex plane fits and, just as for the nylon sample, this was remedied by ex-

trapolating the spectrum somewhat at both high and low values of ϵ'. The fits could have been improved for high frequencies if more data were available. In order to perform a successful fit, it is crucial to have measured the entire minimum in the spectrum.

For both the Nylon-66 and the PVDF data, the parameter points $g_{/\!/}$ seem to be collected quite close to the critical surface of A_2 singularities. This may be due to the fact that the present version of the MCT considers liquid and ideal glass states and that the transition between them takes place in an abrupt manner, manifested in the disappearance of the α peak when crossing the surface from the liquid over to the glassy side. In reality, the crossover between the liquid and glassy states is observed to be smooth, the α peak is present on both sides, and no singular behavior can be seen. This can be accounted for in the MCT by the inclusion of activated hopping processes that serve to smooth out the sharpness of the transition [33,34]. Consequently, some of the parameter points that seem to be collected close to the critical surface may in reality belong to the glassy side.

An A_4 evaluation of data from dielectric measurements on the polymer gel system PAN-EC-PC has been presented elsewhere [16]. Two representative spectra from this earlier investigation are presented in Fig. 5 as an illustration of how well the A_4 fits work in this case. The data from this system show a typical A_4 signature and the polynomial fits produce very good results that are easily carried over to the frequency-plane plots. The range of frequencies over which there is agreement between theory and experiment is in this case rather small, only about 2 decades. It may therefore be argued that given the amount of fitting parameters, five in this case for $\epsilon''(\nu)$, it is not surprising that such good fits are produced. It should however be noted that firstly, the MCT higher-order scenarios predict very distinct and easily recognizable susceptibility spectra. The A_4 scenario can therefore not be used to fit any arbitrary curve. Secondly, because of the scaling properties according to Eqs. (12) and (21), there are in reality only two parameters determining the shape of the entire curve, viz., $\tilde{g}_3$ and $\tilde{g}_4$, see above. Once the shape has been determined, the parameters g_2, g_3, and g_4 are calculated according to

$$g_2 = \pm s^2,$$

$$g_3 = s^3 \tilde{g}_3,$$

$$g_4 = s^4 \tilde{g}_4,$$

where the scaling parameter s has been defined above. Defined in this way, a variation of s will only lead to contraction or expansion of the theoretical curve without changing its shape. The two remaining parameters, ϵ_c and t_1, have no influence on the shape of the curve but will only shift the curve in the vertical or horizontal directions, respectively.

In Fig. 6, data from measurements on PCTFE performed by Scott *et al.* [10] are shown together with their corresponding MCT fits. As for all the other polymers, the A_4 fits produce very good results with correspondence between theory and experiment over a frequency range between 6 and 7 decades. Similar to the PET data, one sample (44% crystallinity at 100 °C) is found to lie very close to the A_3 point in Fig. 1. For illustrational purposes, an A_3 fit was therefore also performed for this spectrum and, as seen in the figure, the A_3 and A_4 functions provide in this case almost identical results.

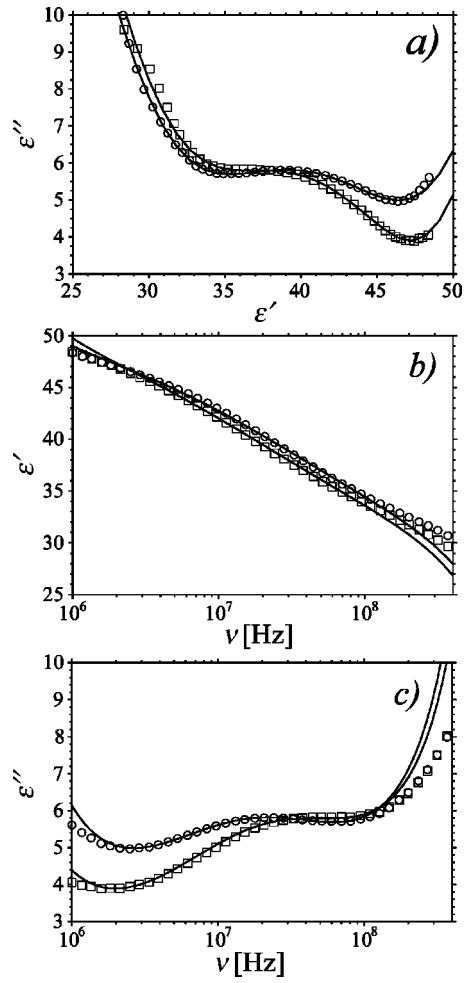

FIG. 5. MCT fits to the dielectric function of the system PAN-EC-PC. Full lines are A_4 fits, see text. (a) Complex-plane plot, (b) real, and (c) imaginary part of the dielectric function plotted as functions of frequency ν. Circles, sample 8 at 35 °C; squares, sample 14 at 43 °C. In Fig. 1, the coordinates $(\tilde{g}_3,\tilde{g}_4)$ of these spectra are $(-0.29,-1.8)$ and $(-0.54,-1.3)$ and the g_2 parameters are 0.12 and 0.14, respectively. Sample numbers are related to the amount of EC and PC in the samples such that a higher number corresponds to a smaller amount of these substances.

Since a number of the spectra from this dataset show A_3-like behavior, it has previously been evaluated within this scenario [11]. It was then found that some of the data followed a scaling line in the A_3 parameter space and it could indeed be shown that the scaling predictions of the theory were found to hold. In the A_4 case, there do exist parameter points (g_2,g_3,g_4) with similar p- and q-values, and a scaling analysis can therefore be performed. The results from this analysis are presented in Fig. 7. In these graphs the data clearly show the predicted scaling behavior. Deviations from the master curves do occur because all the data do not ex-

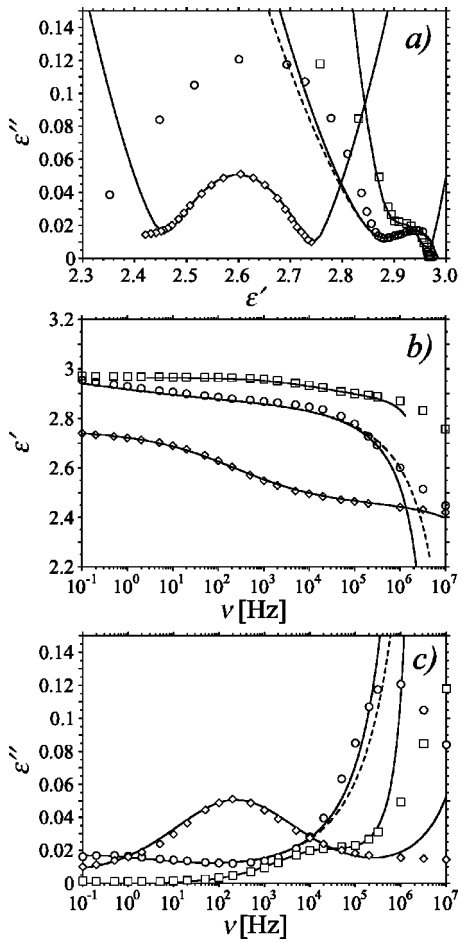

FIG. 6. MCT fits to the dielectric function of PCTFE. Full lines are A_4 fits and dashed lines fits to the A_3 scenario, see text. (a) Complex-plane plot, (b) real, and (c) imaginary part of the dielectric function plotted as functions of frequency ν. Diamonds, 80% crystallinity at 0 °C; circles, 44% crystallinity at 100 °C, squares, 73% crystallinity at 175 °C. In Fig. 1], the coordinates $(\tilde{g}_3,\tilde{g}_4)$ of these spectra are $(-0.012,-0.27)$, $(-0.52,0.069)$, and $(-0.68,-0.78)$ and the g_2 parameters are 0.095, 0.14, and 0.12, respectively.

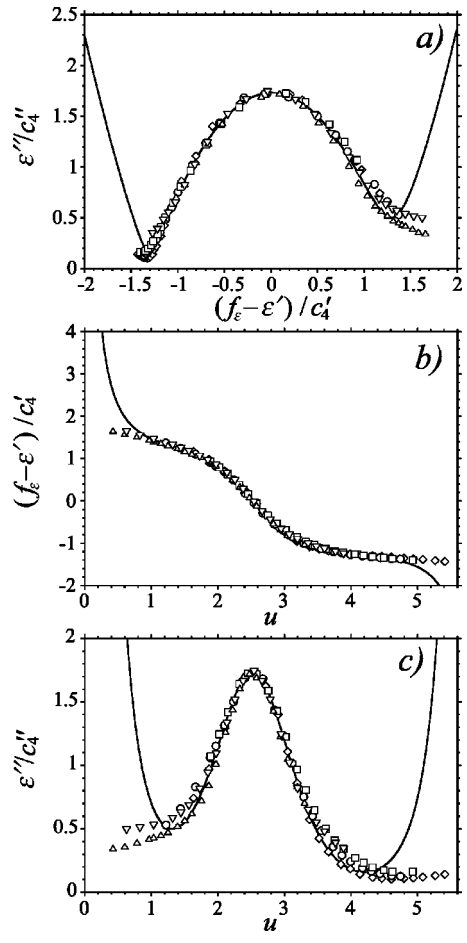

FIG. 7. Rescaled dielectric function of PCTFE. (a) Complex-plane plot, (b) real, and (c) imaginary part of ϵ plotted as functions of $u=-\ln(2\pi\nu t_1)/y_4$. Full lines are the calculated master curves with $p=0.32$ and $q=1.1\times10^{-8}$ according to Eq. (22) for the complex plane plot and Eqs. (14) for the frequency plots. Triangles, 80% crystallinity at -25 °C; inverted triangles, 80% crystallinity at 0 °C, squares, 12% crystallinity at 48 °C; circles, 44% crystallinity at 50 °C; diamonds, 44% crystallinity at 75 °C.

actly follow the scaling line. The temperature dependences of the scaling parameters c_4', c_4'', and $1/y_4$ are shown in Fig. 8. According to Eq. (17b), c_4''/ϵ_c should exhibit a square root dependence. This is shown in Fig. 8(a), in which a fit to Eq. (17b) yields a critical temperature T_0 of -91 °C. This value of T_0 was used as a fixed value when performing the fits in Figs. 8(b) and 8(c). The scattering of the points is, as discussed above, due to that the parameter points $g_{/\!/}$ do not exactly follow the given scaling line. Similar results are obtained for the other parameters c_4' and $1/y_4$, as shown in Figs. 8(b) and 8(c). For these parameters it is possible to perform a consistency check, since

$$\frac{1}{y_4}=\left|\frac{g_4}{3}\right|^{1/4}=\frac{2c_4''}{\pi c_4'} \tag{23}$$

as can be deduced from Eq. (12) and $s=|g_4/3|^{1/4}$. The rightmost relation is especially interesting, since the two parameters c_4' and c_4'' are determined independently from ϵ' and ϵ'', respectively. As shown in the figures, these relations are satisfied to good accuracy. However, due to the lack of points for temperatures close to T_0, the use of a linear function, $f(T)\propto(T-T_0)$, will produce fits of equal quality. The scaling predictions can therefore not be completely verified in this case. The fact that, in contrast to the linear fits, the three fits using Eqs. (17) are consistent, i.e., can be performed using the same parameter T_0, makes it interesting to investigate this open issue further by performing measurements in the temperature range around T_0.

V. SUMMARY AND CONCLUSIONS

The dielectric spectra of polymers are often too complicated to be adequately described by phenomenological models such as the Havriliak-Negami function. As shown in the present work, as well as in earlier reports [11–16], the higher-order mode-coupling scenarios, and especially the A_4

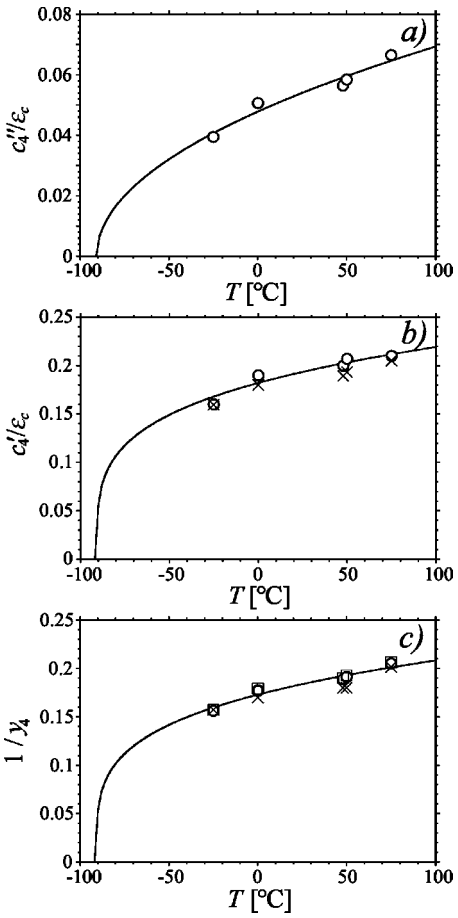

FIG. 8. Scaling parameters extracted from the scaling plots in Fig. 7 versus temperature. (a) c_4'', the full line is the best fit to Eq. (17b) yielding $T_0=-91\,^\circ$C. (b) c_4', full line is the best fit to Eq. (17a) with $T_0=-91\,^\circ$C. Circles, c_4' extracted from experimental data; crosses, c_4' calculated from $c_4'=2c_4''|3/g_4|^{1/4}/\pi$, see text. (c) $1/y_4$, full line is the best fit to Eq. (17c) with $T_0=-91\,^\circ$C. Circles, $1/y_4$ extracted from experimental data; squares, $1/y_4$ calculated from $1/y_4=|g_4/3|^{1/4}$; crosses, $1/y_4$ calculated from $1/y_4=2c_4''/\pi c_4'$.

scenario, are capable of providing a very good description of this type of data. Since the present version of the MCT is derived from a simple monatomic fluid, it may be argued that the theory is not applicable to such complicated systems as polymers. It is however important to understand that the MCT predicts that close to a glass transition singularity the relaxation spectra are independent of the microscopic features of the material under study and are solely determined by the topological features of the parameter space. Accordingly, any future theory for polymers developed out of the MCT framework [35] will produce the same results as presented in this article, provided one can drive the system under study sufficiently close to the relevant singularity.

One might expect it to be quite difficult to find several spectra along one particular scaling line in the A_4 parameter space. In any case, large amounts of data may be needed in order for a scaling analysis to be successful. The PCTFE data presented here nevertheless do contain a sufficient amount of spectra following such a scaling line and a scaling analysis can therefore be performed. The fact that the scaling parameters extracted from this analysis show the expected temperature dependence provides additional support for the theory.

Because of the large amount of data needed, carrying out a MCT A_4 analysis of dielectric data for polymers is a laborious task. In order to cover different parts of the (g_2,g_3,g_4) parameter space it is necessary to vary not just the temperature, but also other properties such as degree of crystallinity, pressure, composition, water content, and so on. The data analysis is facilitated considerably by utilizing the polynomial fits presented in this paper. Care must here be taken so that a wide enough frequency window is used in order to cover as large a part of the minimum in $\epsilon''(\nu)$ as possible.

In experimental studies to date, only dielectric measurements have shown the existence of the higher-order MCT glass transition singularities. It would be highly interesting to investigate whether other experimental techniques would produce similar results, such as, e.g., light-scattering and within this category especially photon correlation spectroscopy, which has a dynamical window covering the frequency range within which the higher-order MCT signatures are present in the dielectric data. Here, the existence of low-frequency artifacts due to free charges do not present a problem and it may therefore be possible to examine the low-frequency behavior of the polymer spectra in greater detail.

ACKNOWLEDGMENTS

The author would like to thank I. Halalay, B.-E. Mellander, and L. Sjögren for providing many helpful comments on the manuscript. This work has received financial support from the Swedish Natural Science Research Council.

[1] K.S. Cole and R.H. Cole, J. Chem. Phys. **9**, 341 (1941).
[2] D.W. Davidson and R.H. Cole, J. Chem. Phys. **18**, 1417 (1950).
[3] D.W. Davidson and R.H. Cole, J. Chem. Phys. **19**, 1484 (1951).
[4] S. Havriliak and S. Negami, J. Polym. Sci., Part C: Polym. Symp. **14**, 99 (1966).
[5] W.O. Baker and W.A. Yager, J. Am. Chem. Soc. **64**, 2171 (1942).
[6] T. Nakajima and S. Saito, J. Polym. Sci. **31**, 423 (1958).
[7] S. Saito and T. Nakayima, J. Appl. Polym. Sci. **2**, 93 (1959).
[8] Y. Ishida, O. Amano, and M. Takayanagi, Kolloid-Z. **172**, 129 (1960).
[9] Y. Ishida, K. Yamafuji, H. Ito, and M. Takayanagi, Kolloid Z. Z. Polym. **184**, 97 (1962).
[10] A.H. Scott, D.J. Scheiber, A.J. Curtis, J.I. Lauritzen, and J.D. Hoffman, J. Res. Natl. Bur. Stand., Sect. A **66**, 269 (1962).
[11] L. Sjögren, J. Phys.: Condens. Matter **3**, 5023 (1991).
[12] S. Flach, W. Götze, and L. Sjögren, Z. Phys. B: Condens. Matter **87**, 29 (1992).

[13] I. Halalay, J. Phys.: Condens. Matter **8**, 6157 (1996).
[14] H. Eliasson, B.-E. Mellander, and L. Sjögren, J. Non-Cryst. Solids **235-237**, 101 (1998).
[15] H. Eliasson and B.-E. Mellander, J. Phys.: Condens. Matter **11**, 8807 (1999).
[16] H. Eliasson, B.-E. Mellander, and L. Sjögren, J. Phys.: Condens. Matter **11**, 10 285 (1999).
[17] W. Götze and L. Sjögren, J. Phys.: Condens. Matter **1**, 4203 (1989).
[18] P. Debye, *Polar Molecules*, 1st ed. (Dover, New York, 1929).
[19] C. J. F. Böttcher, *Theory of Electric Polarization*, 1st ed. (Elsevier, Amsterdam, 1952).
[20] For reviews of the MCT, see, e.g., W. Götze, in *Liquids, Freezing and Glass Transition*, edited by J. P. Hansen, D. Levesque and J. Zinn-Justin (North-Holland, Amsterdam, 1991); W. Götze and L. Sjögren, Rep. Prog. Phys. **55**, 241 (1992); Transp. Theory Stat. Phys. **24**, 801 (1995).
[21] W. Götze, J. Phys.: Condens. Matter **11**, A1 (1999).
[22] R. Gilmore, *Catastrophe Theory for Scientists and Engineers* (Wiley, New York, 1981).
[23] V. I. Arnol'd, *Catastrophe Theory*, 2nd ed. (Springer, Berlin, 1986).
[24] A. Hofmann, F. Kremer, and E.W. Fischer, Physica A **201**, 106 (1993).
[25] M.E. Baur and W.H. Stockmayer, J. Chem. Phys. **43**, 4319 (1965).
[26] M. Fuchs, W. Götze, I. Hofacker, and A. Latz, J. Phys.: Condens. Matter **3**, 5047 (1991).
[27] H. Eliasson, Ph.D. thesis, Göteborg University and Chalmers University of Technology, Göteborg, Sweden, 1999.
[28] D.H. McQueen and M. Safari Ardi, J. Mater. Sci. **31**, 357 (1996).
[29] R. Lovell, J. Phys. C **7**, 4378 (1974).
[30] S. Yano, J. Polym. Sci., Part A-2 **8**, 1057 (1970).
[31] Y. Miyamoto, H. Miyaji, and K. Asai, J. Polym. Sci., Polym. Phys. Ed. **18**, 597 (1980).
[32] G.K. Rashmi and P.K.C. Pillai, J. Mater. Sci. **22**, 2006 (1987).
[33] S.P. Das and G.F. Mazenko, Phys. Rev. A **34**, 2265 (1986).
[34] W. Götze and L. Sjögren, Z. Phys. B: Condens. Matter **65**, 415 (1987).
[35] K.S. Schweizer, Phys. Scr. **T49**, 99 (1993).